ACS MATERIALS Au
AN OPEN ACCESS JOURNAL OF THE AMERICAN CHEMICAL SOCIETY

pubs.acs.org/materialsau
Article

Scalable Production of Peptides for Enhanced Struvite Formation via Expression on the Surface of Genetically Engineered Microbes

Jacob D. Hostert,[‡] Quincy A. Spitzer,[‡] Paola Giammattei, and Julie N. Renner*

Cite This: *ACS Mater. Au* 2023, 3, 548−556
Read Online

ACCESS | Metrics & More | Article Recommendations | Supporting Information

ABSTRACT: A promising method for recycling phosphate from wastewater is through precipitation of struvite ($MgNH_4PO_4{\cdot}6H_2O$), a slow-release fertilizer. Peptides have been shown to increase the yield of struvite formation, but producing peptides via solid phase synthesis is cost prohibitive. This work investigates the effects of peptide-expressing bacteria on struvite precipitation to provide a sustainable and cost-efficient means to enhance struvite precipitation. A peptide known for increased struvite yield was expressed on a membrane protein in *Escherichia coli*(*E. coli*), and then 5 mL precipitation reactions were performed in 50 mL culture tubes for at least 15 min. The yield of struvite crystals was examined, with the presence of peptide-expressing *E. coli* inducing significantly higher yields than nonpeptide-expressing *E. coli* when normalized to the amount of bacteria. The precipitate was identified as struvite through Fourier transform infrared spectroscopy and energy dispersive spectroscopy, while the morphology and size of the crystals were analyzed through optical microscopy and scanning electron microscopy. Crystals were found to have a larger area when precipitated with the peptide-expressing bacteria. Additionally, bacteria−struvite samples were thermogravimetrically analyzed to quantify their purity and determine their thermal decomposition behavior. Overall, this study presents the benefits of a novel, microbe-driven method of struvite precipitation, offering a means for scalable implementation.

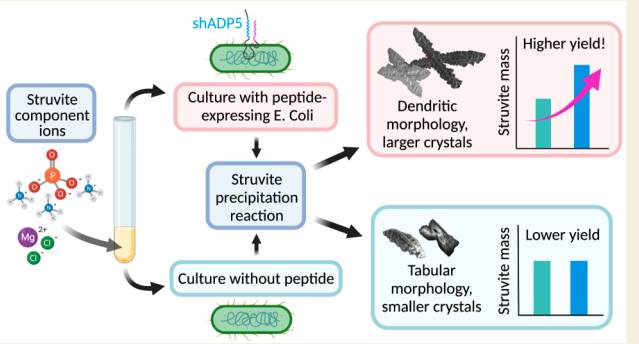

KEYWORDS: *struvite, phosphorus recovery, synthetic biology, crystal growth, amelogenin peptide*

INTRODUCTION

Struvite ($MgNH_4PO_4{\cdot}6H_2O$) is a slow-release fertilizer that readily precipitates at basic pH according to the following equation:

$$Mg^{2+} + NH_4^+ + H_nPO_4^{3-n} + 6H_2O \rightarrow MgNH_4PO_4{\cdot}6H_2O + nH^+ \quad (1)$$

where n = 0, 1, or 2 depending on the solution pH.[1] Struvite precipitation is an attractive way to recover excess phosphate from waste streams,[2−5] with life cycle assessment and budget analysis studies showing the process to be economically viable when combined with recovery of other products.[6−9] Phosphate is a particularly important nutrient, as nearly all phosphate applied as fertilizer is sourced from mined phosphate rock—a resource that is dwindling and expected to cause supply issues by the end of the century.[10]

The slow-release characteristic of struvite is desirable in a fertilizer because it allows for lower amounts of phosphorus runoff. Currently struvite is formed via chemical or electrochemical precipitation from wastewater,[8,11,12] where magnesium typically needs to be supplemented and the pH adjusted to get high struvite yields.[4] Ammonium and phosphate are usually at sufficient concentrations such that no salts need to be added.[13] Adding chemicals (i.e., salts or hydroxide for pH adjustment) increases the cost of the process; however, careful selection of waste streams that have sufficient magnesium content[1] and introducing a biologic process to modulate pH could obviate the need to add chemicals. Struvite precipitation may be coupled with recovery of other valuable products (e.g., hydrogen) to further enhance its economic value and mitigate costs associated with added chemicals.[14,15]

Struvite also naturally forms as bladder stones, usually coupled with infection from *Proteus* species of bacteria.[16−18] The biologically induced precipitation of struvite suggests a potential means to increase struvite formation using biomolecules or microorganisms. Our previous studies have investigated a peptide derived from amelogenin proteins, shADP5,[19] that increases the amount of struvite formation and

Received: May 2, 2023
Revised: June 28, 2023
Accepted: June 29, 2023
Published: July 26, 2023

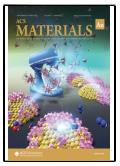

https://doi.org/10.1021/acsmaterialsau.3c00037
ACS Mater. Au 2023, 3, 548−556

induces changes in crystal morphology.[11,20] The primary sequence of shADP5 is SYENSHSQAINVDRT. When coupled with an electrochemical system, surface-bound shADP5 peptides increased struvite production even at neutral pH.[11] Other peptides like polyaspartic acid[21] have also been shown to alter crystal morphology but to the detriment of struvite yield. While peptides are a promising means to increase the yield of struvite, they are often made through chemical synthesis or biological production followed by separation and purification—neither method being particularly low cost. Producing the peptide via bacteria-based platforms without purification has the advantage of being better adapted for scalable systems, with both aerobic and anaerobic digestors being well-established unit operations in wastewater treatment plants. In addition, a study on biologically assisted struvite formation highlights that the metabolism of bacteria can raise pH and mitigate the need to add base.[22] Low-molecular weight peptides naturally produced by bacteria[22] have also been shown to promote struvite growth, but use of sequence-defined peptides in an easily engineered bacterial system for struvite growth remains unexplored.

In this study, we aim to investigate the impact of shADP5 expressed on the surface of *Escherichia coli*(E. coli) on struvite production. To achieve this, we genetically modified *E. coli* such that shADP5 would be tethered to a membrane protein (eCPX[23]) with biterminal peptide display. The biterminal display enables the use of a second peptide, located at the opposite terminus, for detection of expression. This membrane protein system has been used for a variety of applications, including bacteria−nanoparticle hybrid materials,[24] high-affinity peptide screening,[25] and microbial fuel cells,[26] but has not been utilized in the context of struvite precipitation or phosphate recovery. To precipitate struvite, *E. coli* was allowed to grow overnight in the presence of added magnesium or both magnesium and phosphate. The pH was then adjusted to 10 using sodium hydroxide, and the yield of struvite was determined gravimetrically after filtration. The identity of the precipitate was confirmed as struvite through Fourier transform infrared spectroscopy (FTIR) and energy dispersive spectroscopy (EDS). The proportion of struvite to organic content was characterized via thermogravimetric analysis (TGA). The morphology of struvite crystals was also examined and quantified using both optical microscopy and scanning electron microscopy (SEM). Overall, this study tests the hypothesis that shADP5 enhances struvite precipitation when surface-bound to microbes, which will help shape an economically viable process for struvite production.

MATERIALS AND METHODS

Materials

Deionized (DI) water (H_2O) was used throughout the study and was generated via a mixed bed deionizer tank from Western Reserve Water Systems (1−10 MΩ). Ammonium phosphate monobasic ($NH_4H_2PO_4$, 98%) and magnesium chloride hexahydrate ($MgCl_2 \cdot 6H_2O$, 99.0−102%) were obtained from VWR. Hydrochloric acid (HCl, 1 N) and sodium hydroxide pellets (NaOH) for pH adjustment were obtained from Fisher Chemical. Poly(vinylidene fluoride) (PVDF) membranes (47 mm, 0.45 μm) were obtained from MilliporeSigma. Powdered LB media was obtained from Fisher Chemical. Agar was obtained from VWR. Arabinose was obtained from Alfa Aesar. Chloramphenicol was obtained from DOT Scientific. Tris was obtained from DOT Scientific. NaCl was obtained from Fisher Chemical. Streptavidin, *R*-phycoerythrin conjugate (SAPE), super optimal broth with catabolite repression (SOC) medium and chemically competent MC1061 *E. coli* were obtained from Invitrogen. Powdered Luria−Bertani (LB) medium was obtained from Fisher Chemical. Ethanol (200 proof) was obtained from Sigma-Aldrich. The shADP5 containing eCPX plasmid was obtained from Genscript, and pB33eCPX was a gift from Patrick Daugherty (Addgene plasmid # 23336; http://n2t.net/addgene:23336; RRID: Addgene_23336). Polystyrene cuvettes were obtained from MilliporeSigma.

Plasmid Construction

Two plasmids were designed to express eCPX membrane proteins. The first plasmid was the unmodified membrane protein, pB33eCPX—referred to in this study as MEMP. This plasmid was used to assess the impacts of bacteria and expression of the membrane protein (eCPX) on struvite precipitation. The second plasmid, referred to as MDEN in this study, was designed to express the shADP5 peptide on the C-terminus and a fluorophore-binding peptide consisting of a streptavidin−*R*-phycoerythrin (SAPE) tag (primary sequence: AECHPQGPPCIEGRK, which binds streptavidin−*R*-phycoerythrin fluorophore, SAPE[23]) on the N-terminus of eCPX. Codons were optimized using Benchling software for MDEN. Both plasmids contained genes for chloramphenicol resistance, and eCPX was under the control of the L-arabinose operon. The combination of these genes allows for selection of successfully transformed bacteria and selective expression of eCPX (and peptide tags in the case of MDEN) depending on whether or not arabinose is introduced, respectively. Plasmid sequences may be found in the Supporting Information. An illustration of expressed MDEN and MEMP is shown in Figure 1.

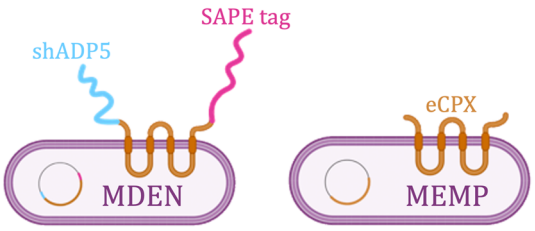

Figure 1. Cartoon representations of the different plasmids transfected into *E. coli* used in this study, MDEN (expressing the membrane protein shown in orange, sHADP5 peptide shown in blue, and SAPE tag shown in pink) and MEMP (expressing only the membrane protein shown in orange).

Transfection

E. coli cells were transfected with either MDEN or MEMP plasmids. To transfect the cells, LB agar plates were prepared with 0.025 mg/mL of chloramphenicol to select for the antibiotic resistance introduced with the plasmids. The plasmid DNA (MDEN and MEMP) was centrifuged at 6000 × *g* and then vortexed for 1 min with 20 μL of DI water. A volume of 2 μL of DNA solution was added to 100 mL of chemically competent *E. coli* cells. These cells were incubated on ice for 30 min and then heat shocked at 42 °C for 30 s using a dry block heater and then placed in ice for an additional 2 min. SOC medium (900 μL) was added to each tube. The transfected cells were incubated for 60 min at 37 °C and shaken at 225 rpm. These clones were spread into LB agar plates with 0.025 mg/mL chloramphenicol and incubated overnight at 37 °C. Single colonies were grown up and stored at −80 °C in a solution of 50% glycerol and 50% DI water as glycerol stocks.

Fluorescent Assay

To establish that the cells expressed the membrane proteins with a peptide tag, a fluorescent assay was performed using a 96-well plate. To eliminate any source of contamination, the wells were washed 25 times with 240 μL of deionized water using a multichannel electronic pipet and dried with nitrogen gas. After overnight expression (see Bacterial Culture and Struvite Precipitation), 10 μL of induced and uninduced cells was labeled with streptavidin−*R*-phycoerythrin

https://doi.org/10.1021/acsmaterialsau.3c00037
ACS Mater. Au 2023, 3, 548−556

(SAPE) and incubated in a dark room at 4 °C. The cells incubated with the fluorophore were centrifuged for 3 min at 17.8 × *g*. The supernatant was collected, and the cell pellets were resuspended in 300 μL of phosphate-buffered saline (PBS). Samples of 150 μL of induced and uninduced cells resuspended in PBS were added to the wells, and the fluorescence intensity was measured using a Spectramax M2 plate reader at an excitation wavelength of 496 nm and an emission wavelength of 578 nm.

Solution Preparation for Bacterial Expression and Struvite Precipitation

Tubes filled with LB medium were prepared by combining LB powder with DI water in a 1:50 ratio. Glass culture tubes were filled with 5 mL of the LB solution and then autoclaved for sterilization.

Three stock solutions were prepared prior to struvite precipitation. A 1 M magnesium solution was made using DI water and $MgCl_2 \cdot 6H_2O$. Similarly, a 2 M ammonium phosphate solution was prepared from DI water and $NH_4H_2PO_4$. A 4% arabinose solution was made by vortexing 96 mg of arabinose powder into 2.4 mL of DI water until completely dissolved and then sterile-filtering into a sterile 2 mL Eppendorf tube.

Bacterial Culture and Struvite Precipitation

To begin bacterial culture, two LB agar plates containing 0.025 mg/mL chloramphenicol and 0.0004 g/mL arabinose were streaked with each of the clones under study from a glycerol stock to make one MDEN plate and one MEMP plate. The plates were then incubated overnight at 37 °C to allow for colony formation. Post incubation, one colony of each clone was picked via pipet and injected into two sterile tubes each filled with 5 mL LB medium and then incubated overnight at 37 °C and 225 rpm to create a liquid starter culture.

Bacteria were then transferred from the starter culture to a struvite culture. Struvite cultures consisted of six different solutions with varying concentrations of ions, nutrients, and bacteria in tubes containing 5 mL liquid LB medium. All tubes contained 5 μL of 20% chloramphenicol, 17.5 μL of 1 M $MgCl_2$, and 50 μL 0.04 g/mL of arabinose. Varying amounts of ammonium phosphate and bacteria were then added according to Table 1. Control experiments consisting of no bacteria and bacteria with no peptide tags were conducted in samples 1−2 and 5−6, respectively. Once all tubes were prepared, they were incubated overnight at 37 °C and shaken at 225 rpm.

Table 1. Summary of Experimental Conditions for Struvite Culture[a]

Sample	2 M $NH_4H_2PO_4$ 17.5 μL	MDEN *E. coli* 20 μL	MEMP *E. coli* 20 μL
1—no bacteria, no ammonium phosphate			
2—no bacteria, with ammonium phosphate	Y		
3−MDEN bacteria, no ammonium phosphate		Y	
4−MDEN bacteria, with ammonium phosphate	Y	Y	
5−MEMP bacteria, no ammonium phosphate			Y
6−MEMP bacteria, with ammonium phosphate	Y		Y

[a]The contents of struvite sample tubes are described. "Y" indicates the additive shown in the header row was added to the sample. The final concentration of $NH_4H_2PO_4$ in the samples indicated was 7 mM. The final concentration of MDEN *E. coli* and MEMP *E. coli* in samples indicated was 4 μL cells/mL.

After overnight incubation, 150 μL of 1 M NaOH was added to each struvite culture tube to bring the pH to 10 and induce struvite precipitation. Tubes were then agitated for 5 s upon addition of the sodium hydroxide to ensure homogeneous distribution. After agitation, the tubes were allowed to stand for 15 min. All tubes were given equal amounts of time for precipitation. After precipitation, samples were vacuum filtered through 0.22 μm Nylon 6,6 membranes and rinsed with ethanol to avoid dissolving the struvite crystals. Figure S1 shows a diagram of the experimental procedure.

Optical Microscopy

Directly after crystal precipitation, samples were prepared for microscopy. After the precipitation reactions, 200 μL of sample was extracted from each culture tube and injected directly into a clear flat-bottomed 96-well plate. A Tris-buffered saline solution (150 mM NaCl, 50 mM Tris) was used to dilute the sample concentrations in the subsequent rows of the plate for imaging in the case that the undiluted samples had too high of an optical density. The buffer solution was prepared by mixing 4.383 g of Tris, 3.0275 g of NaCl, and 500 mL of DI water. An electronic multichannel pipet was used to add buffer and perform serial dilutions 1:1.

The 96-well plate was imaged on a Leica DMI6000 inverted microscope with a well plate stage holder. Images were collected on samples with no bacteria, samples with MEMP clones, and samples with MDEN clones. Three separate batches (cultured at different times) of each sample type were imaged. Analysis of images was done using ImageJ software. Each crystal was manually traced to determine the area, perimeter, and Feret diameter. All results were recorded in Excel for statistical analysis.

Optical Density at 600 nm (OD 600) Measurements

For measurements of bacterial growth, 2 mL of the solution was pipetted into polystyrene cuvettes with a 1 cm path length. Absorbance was then measured at 600 nm with LB medium serving as the blank on a Nanodrop UV−vis spectrophotometer.

Sample Drying

Immediately following vacuum filtration precipitates were stored in a Thermo Scientific MaxQ 6000 Incubated Stackable Floor Shaker at 30 °C to dry overnight. The dry precipitate was characterized by measuring mass and analyzing via attenuated total reflectance Fourier transform infrared spectroscopy (ATR-FTIR), scanning electron microscopy (SEM), energy dispersive spectroscopy (EDS), and thermogravimetric analysis (TGA).

Fourier Transform Infrared Spectroscopy

The dry precipitate was characterized using attenuated ATR-FTIR on a Nicolet iS50 FT-IR (Thermo Scientific, USA) with a diamond crystal. Data were collected from 400 to 4000 cm^{-1} with 4 cm^{-1} resolution over 32 scans. The collected spectra were normalized to the maximum peak using Omnic 9 software, version 9.8.372 (Thermo Scientific, USA). The struvite crystals were analyzed on the Nylon membrane filters to minimize sample disturbance during data collection. FTIR was chosen to identify struvite in this study as it has been in other studies.[27−31] The collected spectra were then compared to a struvite standard from the RRUFF database.[32]

Scanning Electron Microscopy and Energy Dispersive Spectroscopy

A small amount of dried precipitate was gently scraped off the membrane with a sterile spatula and dusted onto a 0.125″ aluminum stub covered in double-sided carbon tape. Due to the nonconductivity of struvite, samples were then sputter coated with palladium at 30 mTorr for 30 s on a Denton Vacuum Desk IV TSC Sputter Coater. All samples were analyzed on a ThermoFisher Scientific Apreo2 Scanning Electron Microscope with a Schottky field emission gun at a 10 mm working distance.

Energy dispersive spectroscopy was performed on field emission scanning electron microscopy (FESEM) samples using a standard Everhart−Thornley detector. Three points on each representative crystal were examined, with full scale X-ray counts between 40 000 and 101 000 for each point to ensure statistical significance. Pathfinder software was then used to generate EDS spectra with the following specifications: 10 s frame time, 80 s live time limit, 100 eV low-energy cutoff, 20 keV high-energy cutoff.

https://doi.org/10.1021/acsmaterialsau.3c00037
ACS Mater. Au 2023, 3, 548−556

Thermal Gravimetric Analysis

Dried samples were analyzed on a TGA Q500 (TA Instruments). Each sample underwent a ramped heating cycle from 20 to 700 °C at a rate of 20 °C/min. Heating was done on a platinum pan in a nitrogen atmosphere, with a balance purge flow of 20 mL/min and a sample purge flow of 40 mL/min. Three runs were completed on each sample, and crystals from both peptide- and nonpeptide-expressing bacteria were analyzed. Derivative curves were calculated from the change of weight percent with temperature using Python and Excel. The TGA data was used to estimate the purity of the dried precipitate samples and quantify the percentage of bacteria matter and struvite.

Statistical Analysis

Statistical hypothesis testing was performed using Minitab with α = 0.05. For turbidity data (OD 600) as well as struvite crystal area and mass measurements, the equal variance assumption was evaluated *via* Levene's test. If equal variance was violated, Welch's test was conducted to determine if there were significant differences between means followed by the nonparametric Games–Howell *post hoc* test to determine statistical groupings. If equal variance could be assumed, analysis of variance (ANOVA) was performed to determine if there were significant differences between means followed by Tukey's *post hoc* test to determine statistical groupings.

RESULTS AND DISCUSSION

Expression and Detection of Membrane Proteins

The membrane proteins in this study are under the control of the arabinose operon, and thus cells need an arabinose source for their expression. First, growth curve data was recorded along with culture pH and is shown in Figure 2 for a culture of peptide-expressing bacteria (containing the MDEN plasmid, dubbed MDEN bacterial clone). We note that to obtain the growth curve data in Figure 2 the protocol was similar to that of the liquid starter cultures except that arabinose was added after ~200 min. The pH remained close to 7 for the duration of the growth curve, with minimal deviation in pH with time. After the growth characteristics of MDEN bacteria were understood, fluorescent assays to determine successful membrane protein expression were performed—shown in Figure S2. One of the peptide tags on eCPX has strong affinity for the SAPE fluorophore. Typical analysis to determine the expression of this peptide involves sorting *via* flow cytometry;[23] however, we employ a novel fluorescent assay in this study. After incubating, centrifuging, and rinsing both induced and uninduced cultures with SAPE, fluorescence was measured. For uninduced cultures, the fluorescence was an order of magnitude lower than that of induced cultures. This indicates that no fluorophore was strongly bound when no peptides were expressed. The higher fluorescence in induced cultures indicates the successful expression of the SAPE binding tag—the fluorescence remains with the cells during centrifugation and rinsing. Overall, the data using a new fluorescent technique indicate the membrane protein and peptide tags were successfully expressed.

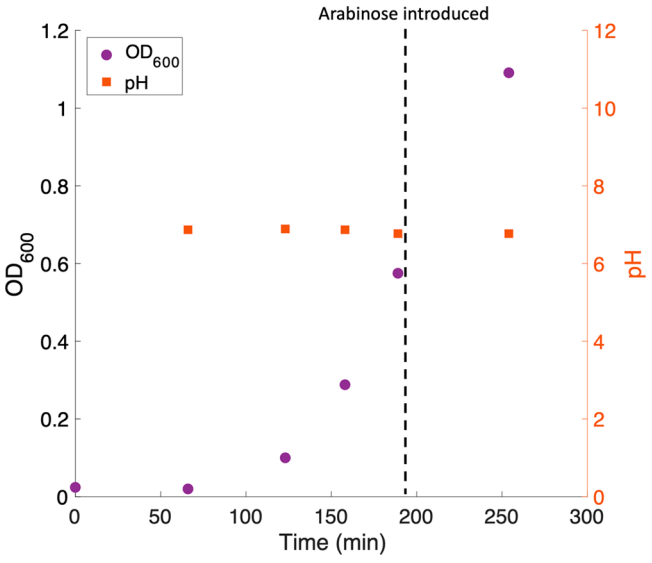

Figure 2. Growth curve of MDEN bacteria. The OD_{600} (purple circles, left axis) represents the turbidity of the medium and is proportional to the growth of bacteria. The pH (orange squares, right axis) is measured as well. Arabinose is added at OD_{600} = 0.5 - 0.6.

Sample Characterization via FTIR and EDS

After successful expression was confirmed, bacterial cultures were used to precipitate struvite. The precipitate was filtered from the medium *via* vacuum filtration. Samples were analyzed using a combination of attenuated total reflectance Fourier transform infrared spectroscopy (ATR-FTIR) and energy dispersive spectroscopy (EDS) to confirm their chemical identity. On all FTIR spectra, characteristic struvite peaks were observed. Specifically, the peaks at 570 and 1000 cm^{-1} are attributed to phosphate in the compound, the peak around 1450 cm^{-1} is associated with water and ammonium ion vibrations, and the broader, asymmetrical peak at 2800 cm^{-1} is attributed to OH/NH bond stretching in the water and ammonium molecules of the crystal, shown in Figure 3a.[20] All other visible peaks are from the Nylon membrane backing. Note that the spectra shown in Figure 3a is gathered from struvite precipitated in the presence of MDEN *E. coli* (composition 4 from Table 1, expressing shADP5 on the surface).

EDS analysis was similarly used to characterize all samples. The spectra generated from scanning each crystal displayed the expected peaks of oxygen, magnesium, and phosphorus representative of struvite crystals (Figure 3b). Nitrogen is likely also present as determined by the software, but its predicted peak is obscured by the oxygen peak.

From the quantitative EDS data generated from struvite samples precipitated in the presence of MDEN *E. coli* (composition 4 from Table 1, expressing shADP5 on the surface), we confirm the individual crystals of precipitate as struvite by examining atomic percentages of each element present in the sample, as shown in Table 2. The Mg:P:O ratio of atomic percent normalized to magnesium is 1:1.32:3.31, while the Mg:P:O ratio of struvite is 1:1:10. Oxygen is difficult to measure quantitatively through EDS due to its production of low-energy X-rays,[33] contributing to the difference between theoretical and measured elemental compositions. Additionally, the vacuum produced during sputter coating and SEM may have dehydrated the crystals, and dehydrated struvite would give a theoretical Mg:P:O ratio of 1:1:4, which is closer to what was observed experimentally. We hypothesize that further deviations of the measured ratio from struvite could be due to the bacterial debris observed upon filtration.

Morphology Analysis via Optical Microscopy and SEM

Precipitated struvite crystals were imaged on carbon tape after being sputter coated with palladium (Figure 4). As seen in Figure 4b, samples precipitated with MDEN bacteria solutions (i.e., expressing shADP5 on the surface) consistently display

https://doi.org/10.1021/acsmaterialsau.3c00037
ACS Mater. Au 2023, 3, 548–556

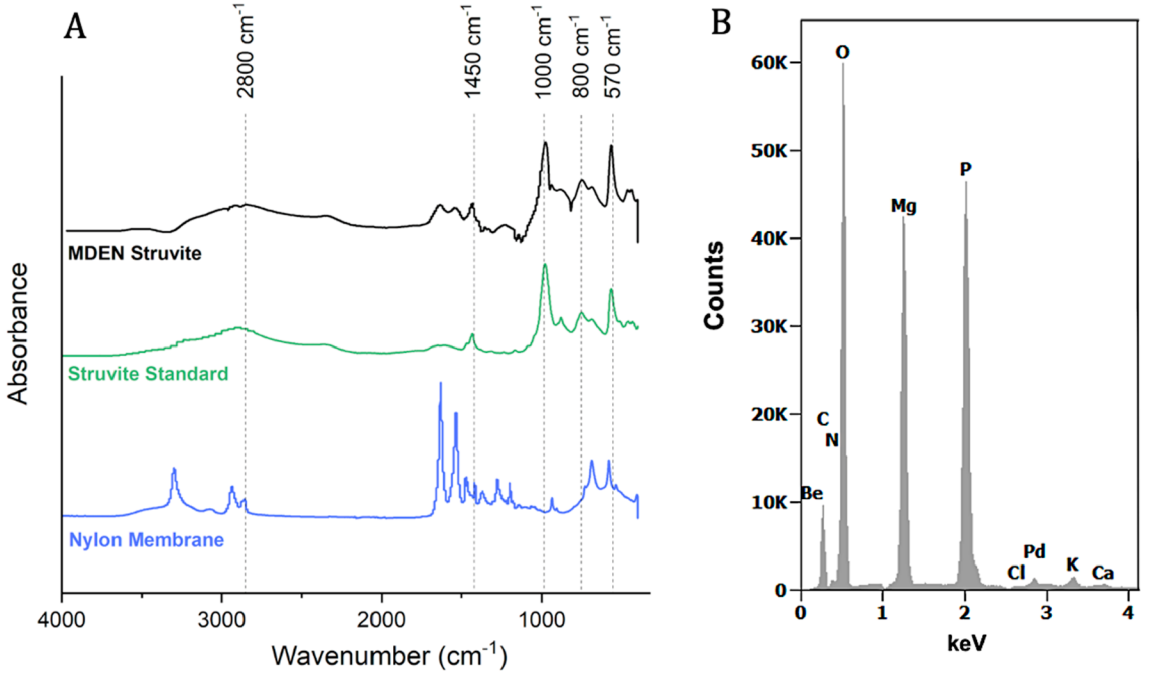

Figure 3. Spectra obtained from struvite precipitated from a MDEN bacterial solution with added ammonium phosphate. (A) ATR-FTIR spectra for the sample, with transmittance normalized to a maximum value of 1. (B) EDS spectra showing the elemental composition of a single crystal.

Table 2. Atomic Composition of a Struvite Sample Precipitated from an Overnight Struvite Culture with Composition 4 in Table 1

Element	Average Compostion (%)
Mg	18
P	23
O	58

feathery or dendritic morphology associated with higher supersaturation.[34] Alternatively, as shown in Figure 4a, the samples precipitated with MEMP bacteria appear bulky and tabular, characteristic of lower supersaturation.[34] The crystals precipitated in cultures using composition 6 (see Table 1—no peptide tags expressed) are also consistently smaller than those precipitated using composition 4 (see Table 1—peptide tags expressed). Figure S3 shows an SEM image of struvite created without bacteria for comparison, demonstrating that smaller crystals generally occur without bacteria present. Overall, the morphological differences seen in Figure 4 provide evidence that the peptide may function by influencing local supersaturation—a phenomena we proposed was happening in our previous work through molecular simulations.[11] Larger crystals could be beneficial in scaled-up systems due to ease of separation from bacteria. Morphology has been linked to dissolution kinetics, with dendritic crystals dissolving faster than tabular crystals, so controlling morphology may become important when designing fertilizer.[35] The dendritic shape observed in this study is also seen in systems using artificial urine and *Proteus mirabilis*;[36,37] however, systems using

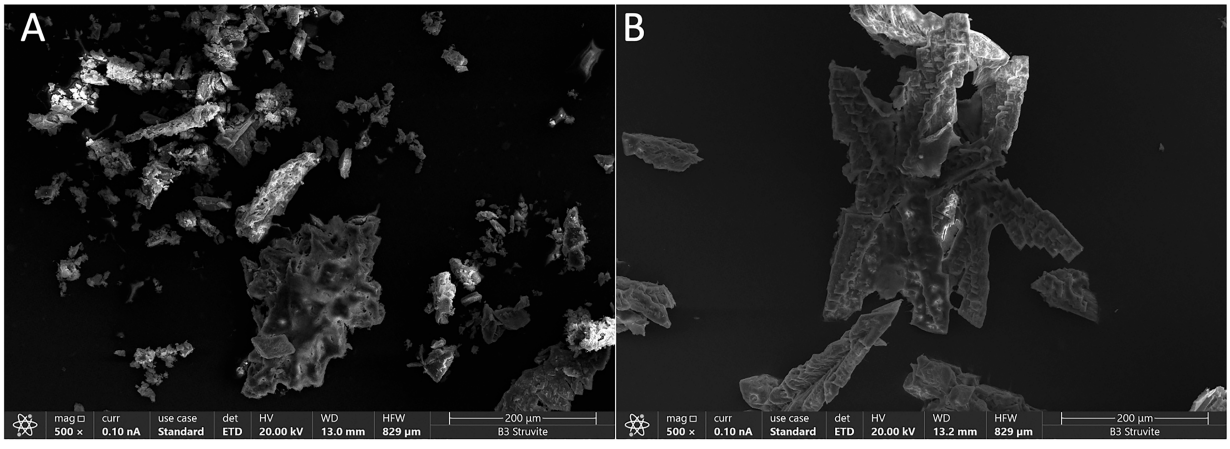

Figure 4. SEM images of struvite samples on an adhesive carbon tab, illustrating differences between precipitation compositions. (a) Struvite precipitated with a nonpeptide-expressing bacterial sample (MEMP cultured under condition 6 in Table 1) at 500× magnification. (b) Struvite precipitated with a peptide-expressing bacterial sample (MDEN cultured under condition 4 in Table 1) at 500× magnification, showing a larger X-shaped and more feathered morphology.

https://doi.org/10.1021/acsmaterialsau.3c00037
ACS Mater. Au 2023, 3, 548−556

Shewanella oneidensis in LB medium showed more tabular morphology.[22,38] The difference in morphology between this study and studies utilizing other bacterial species may be due to the generation of different metabolic products (e.g., low-molecular weight peptides[22] or low-molecular weight organics[39]).

To further evaluate the morphological differences between struvite precipitated in MDEN bacteria cultures and MEMP bacterial cultures, the crystals were imaged in solution *via* bright-field microscopy. Images corroborated the SEM data, with the peptide-expressing samples showing larger, more dendritic morphology (Figure S4).

To compare the crystal sizes of the bright-field microscopy samples, crystal areas were manually traced using ImageJ software to obtain the perimeter, area, and Feret diameter as in our previous work.[20] Crystals with areas greater than 10 000 μm^2 were deemed aggregates and removed from the data set. Final area data gathered from four different samples were analyzed via Minitab: struvite precipitated with peptide-expressing bacteria with no ammonium phosphate added (MDEN, condition 3 in Table 1), peptide-expressing bacteria with ammonium phosphate added (MDEN condition 4 in Table 1), bacteria that did not express peptide with no ammonium phosphate added (MEMP condition 5), and bacteria that did not express peptide with ammonium phosphate added (MEMP condition 6). The assumption of equal variance was tested *via* Levene's test, showing an equal variance assumption to be violated. Welch's test was then conducted without assuming equal variances with a resulting p-value of 0.000 indicating a significant difference (Table S1). The Games–Howell *post hoc* test then was performed to analyze statistical difference between means, with the results showing that samples precipitated in the presence of peptide-expressing bacterial solutions have significantly larger area than their nonpeptide counterparts (Figure 5). A summary of the *post hoc* statistical test used is shown in Table S2. In addition, the presence of ammonium phosphate more than doubled the crystal size for both bacterial samples, likely due to higher supersaturation resulting from the greater concentration of crystallizable ions. Overall, the combined microscopy results and quantitative size measurements suggest that the presence of the shADP5 peptide has a positive effect on precipitating struvite that cannot be accounted for by *E. coli* alone.

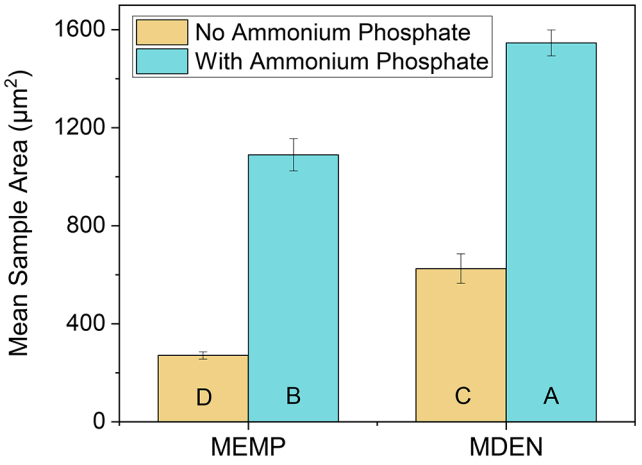

Figure 5. Measured areas of struvite crystals vary depending on the presence of bacterial clones in solution. Letters indicate Games–Howell mean groupings. Data are represented by the mean ± standard deviation. Statistical testing and sample sizes can be found in Tables S1 and S2.

Effect of Peptide-Expressing Bacteria on Struvite Yield

After the struvite cultures were rinsed, filtered, and dried, the mass of struvite was recorded. Figure 6a shows the results for each struvite culture condition (1–6 in Table 1), with detailed statistical results shown in Table S3. The results indicate that the presence of the bacteria has a significant impact on struvite yield, however, the impact of the peptide is unclear. In our previous study in simple solutions, the peptide had reduced impact on yield when lower amounts of struvite seed crystals were present.[20] Additionally, in another study we found an ~20% increase in yield when the peptide was surface-bound compared to without peptide.[11] The error was sufficiently high in this experiment to mask a 20% yield increase. It was also observed that samples contained different amounts of debris post filtering (see Figure S5 for an example photograph). Therefore, TGA was conducted on samples of MEMP and MDEN with ammonium phosphate (see Table S5 and Figure S6) to determine relative amounts of organic material present. This technique also serves to assess purity of the sample. The data indicate that with simple filtration and an ethanol rinse, similar end point weight fractions are observed among samples with bacteria and without bacteria (pure struvite). The bacterial samples were estimated to be at least 95% struvite (Table S5). TGA showed that samples cultured with MEMP bacteria potentially had more bacterial debris than samples cultured with MDEN. To determine how much bacteria was present in samples 3–6 (see Table 1), we measured the OD 600 of each solution after incubation. A higher OD 600 was observed in MEMP samples than in MDEN samples (Table S6). Using the measured OD 600, mass yield data was normalized to the amount of bacteria present, shown in Figure 6b, with detailed statistical information shown in Table S4. We observed a higher yield for MDEN-containing samples when normalized. This indicates that the peptide is likely still playing an integral role in struvite precipitation and that the similarity of the MDEN and MEMP results in Figure 6a are due to differences in the amount of bacteria present. We can predict the amount of struvite and other potential precipitates using the salts added in Table 1. By running a simulation in Visual MINTEQ 3.1 software, it was found that 4.1 mg of struvite was predicted to form—a value that closely matches the results in Figure 6a. Additionally, only struvite was predicted to form as a precipitate in the range of pH simulated, with highest yield seen at pH 10 or higher (Figure S7). The amount of struvite formed is relatively insensitive to pH at a pH of 10 ± 0.5, where a maximum yield is obtained. Since our experiments precipitate at pH 10, local changes in pH are not the likely cause for the increase in yield observed in this study. Higher yields of struvite seen in the bacteria samples could be due to metabolic byproducts (i.e., low -molecular weight compounds) increasing supersaturation and thus yield. Overall, the results shown in Figure 6 highlight the potential for this peptide to positively impact struvite yield and the need to further optimize the bacterial system. For example, trade-offs may occur between peptide production and bacterial replication, which both positively influence struvite yield.

https://doi.org/10.1021/acsmaterialsau.3c00037
ACS Mater. Au 2023, 3, 548–556

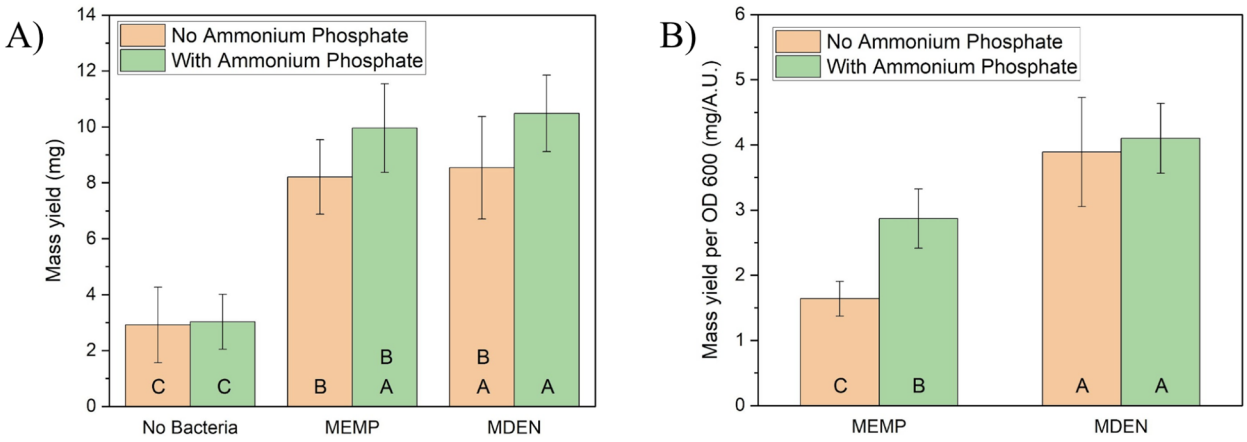

Figure 6. Mass yield of struvite for each sample bacteria type. (A) Direct gravimetric measurements. (B) Gravimetric measurements normalized by the OD 600 measured for each sample. Letters represent the results of a Tukey's (part a) or Games–Howell (part b) *post hoc* test, and bars that do not share a letter are statistically different. Data are represented by the mean ± standard deviation. Sample sizes can be found in Table S3 and Table S4.

CONCLUSION

Overall, a bacterial system to express shADP5 on the surface of *E. coli*was implemented using a membrane protein with biterminal peptide display. After verifying successful expression, impacts of peptide on struvite morphology and yield were examined. Precipitates were first confirmed as struvite through FTIR and SEM-EDS. A more feathery, dendritic morphology was seen when shADP5 was present, in stark contrast to the more tabular struvite crystals seen when shADP5 was absent. This is a clear result of expressing shADP5, not simply an impact of more bacteria, as equal or higher amounts of bacteria are present in samples without shADP5. The crystals precipitated in the presence of shADP5 on the surface of *E. coli*were also significantly larger than crystals precipitated in the presence of*E. coli*that did not express shADP5. The morphological differences in the samples suggested a potential mechanism of action for the peptide where it impacts local supersaturations. The yield of struvite, determined gravimetrically, was positively influenced by the presence of bacteria. When normalized to the amount of bacteria, more struvite was precipitated when shADP5 was expressed. These results set the stage for future work to expand the use of this system in multiple ways. Of particular interest is demonstration of this system in real wastewater to determine if this methodology could be implemented to generate struvite as a byproduct of water treatment. Additionally, there is evidence that struvite precipitates at more neutral pH, particularly in electrochemical systems,[11,40] suggesting future bioelectrochemical applications may be of interest in combination with this or another bacterial platform. Other peptides, or pairs of peptides that work together synergistically, could also be explored for struvite production in this system. To identify other peptides, a peptide library could be constructed and analyzed through the high-throughput method developed in our previous work.[20] Future work will focus on further optimization, scale-up, and economic analysis of the bacterial system investigated in this study. Overall, the system explored in this study is a viable way to implement peptides for scalable biomolecule-enhanced struvite production—without sacrificing the struvite-enhancing properties of the peptide.

ASSOCIATED CONTENT

Supporting Information

The Supporting Information is available free of charge at https://pubs.acs.org/doi/10.1021/acsmaterialsau.3c00037.

Schematic of experimental workflow, fluorescent assay results, supplemental SEM image, optical microscopy images, tables of statistical test outputs, pictures of precipitates, TGA curves, results of MINTEQ simulation with varying pH, raw DNA sequences of plasmids, and DNA sequences (PDF)

Annotated DNA sequence of the MDEN plasmid (PDF)

Annotated DNA sequence of the MEMP plasmid (PDF)

AUTHOR INFORMATION

Corresponding Author

Julie N. Renner − *Department of Chemical and Biomolecular Engineering, Case Western Reserve University, Cleveland, Ohio 44106, United States;* orcid.org/0000-0002-6140-4346; Email: julie.renner@case.edu

Authors

Jacob D. Hostert − *Department of Chemical and Biomolecular Engineering, Case Western Reserve University, Cleveland, Ohio 44106, United States;* orcid.org/0000-0003-3519-7002

Quincy A. Spitzer − *Department of Chemical and Biomolecular Engineering, Case Western Reserve University, Cleveland, Ohio 44106, United States;* orcid.org/0009-0009-3107-1403

Paola Giammattei − *Department of Chemical and Biomolecular Engineering, Case Western Reserve University, Cleveland, Ohio 44106, United States*

Complete contact information is available at: https://pubs.acs.org/10.1021/acsmaterialsau.3c00037

Author Contributions

‡J.D.H. and Q.S. contributed equally. The manuscript was written through contributions of all authors. All authors have given approval to the final version of the manuscript. CRediT: **Jacob D. Hostert** conceptualization (equal), investigation

https://doi.org/10.1021/acsmaterialsau.3c00037
ACS Mater. Au 2023, 3, 548−556

(equal), writing-original draft (equal); **Quincy A. Spitzer** investigation (equal), writing-original draft (equal); **Paola Giammattei** investigation (equal), writing-original draft (equal); **Julie N. Renner** conceptualization (equal), funding acquisition (equal), project administration (equal), writing-original draft (equal).

Notes

The authors declare no competing financial interest.

■ ACKNOWLEDGMENTS

This work was supported by the United States Department of Agriculture (Award No. 2018-68011-28691) as well as the National Science Foundation, EEC Division of Engineering Education and Centers, NSF Engineering Research Center for Advancing Sustainable and Distributed Fertilizer production (CASFER), NSF 20-553 Gen-4 Engineering Research Centers award #2133576 and Division of Chemistry, Track 3 INFEWS award #1739473. Any opinions, findings, and conclusions or recommendations expressed in this material are those of the author(s) and do not necessarily reflect the views of the National Science Foundation. Case Western Reserve University (CWRU) also supplied funding for Q.S. and P.G. through the SOURCE program. We also thank the CWRU Swagelok Center for Surface Analysis of Materials for their guidance in using SEM-EDS, and the CWRU Department of Macromolecular Science and Engineering for allowing us to utilize their TGA apparatus. We would also like to acknowledge BioRender.com for providing the illustration software used to create the table of contents image.

■ REFERENCES

(1) Le Corre, K. S.; Valsami-Jones, E.; Hobbs, P.; Parsons, S. A. Phosphorus Recovery from Wastewater by Struvite Crystallization: A Review. *Critical Reviews in Environmental Science and Technology* **2009**, *39* (6), 433−477.

(2) Bouropoulos, N. C.; Koutsoukos, P. G. Spontaneous precipitation of struvite from aqueous solutions. *J. Cryst. Growth* **2000**, *213* (3−4), 381−388.

(3) de-Bashan, L. E.; Bashan, Y. Recent advances in removing phosphorus from wastewater and its future use as fertilizer (1997−2003). *Water Res.* **2004**, *38* (19), 4222−4246.

(4) Doyle, J. D.; Parsons, S. A. Struvite formation, control and recovery. *Water Res.* **2002**, *36* (16), 3925−3940.

(5) Doyle, J. D.; Philp, R.; Churchley, J.; Parsons, S. A. Analysis of struvite precipitation in real and synthetic liquors. *Process Safety and Environmental Protection* **2000**, *78* (B6), 480−488.

(6) Brye, K. R.; Omidire, N. S.; English, L.; Parajuli, R.; Kekedy-Nagy, L.; Sultana, R.; Popp, J.; Thoma, G.; Roberts, T. L.; Greenlee, L. F. Assessment of Struvite as an Alternative Sources of Fertilizer-Phosphorus for Flood-Irrigated Rice. *Sustainability* **2022**, *14* (15), 9621.

(7) Morrissey, K. G.; English, L.; Thoma, G.; Popp, J. Prospective Life Cycle Assessment and Cost Analysis of Novel Electrochemical Struvite Recovery in a US Wastewater Treatment Plant. *Sustainability* **2022**, *14* (20), 13657.

(8) Omidire, N. S.; Brye, K. R.; English, L.; Popp, J.; Kekedy-Nagy, L.; Greenlee, L.; Roberts, T. L.; Gbur, E. E. Wastewater-recovered struvite evaluation as a fertilizer-phosphorus source for corn in eastern Arkansas. *Agronomy Journal* **2022**, *114* (5), 2994−3012.

(9) Sena, M.; Hicks, A. Life cycle assessment review of struvite precipitation in wastewater treatment. *Resources Conservation and Recycling* **2018**, *139*, 194−204.

(10) Cordell, D.; White, S. Peak Phosphorus: Clarifying the Key Issues of a Vigorous Debate about Long-Term Phosphorus Security. *Sustainability* **2011**, *3* (10), 2027−2049.

(11) Wu, I.; Hostert, J. D.; Verma, G.; Kuo, M.-C.; Renner, J. N.; Herring, A. M. Electrochemical Struvite Precipitation Enhanced by an Amelogenin Peptide for Nutrient Recovery. *ACS Sustainable Chem. Eng.* **2022**, *10* (43), 14322−14329.

(12) Sultana, R.; Kekedy-Nagy, L.; Daneshpour, R.; Greenlee, L. F. Electrochemical recovery of phosphate from synthetic wastewater with enhanced salinity. *Electrochim. Acta* **2022**, *426*, 140848.

(13) Crutchik, D.; Garrido, J. M. Struvite crystallization versus amorphous magnesium and calcium phosphate precipitation during the treatment of a saline industrial wastewater. *Water Sci. Technol.* **2011**, *64* (12), 2460−2467.

(14) Mayer, B. K.; Baker, L. A.; Boyer, T. H.; Drechsel, P.; Gifford, M.; Hanjra, M. A.; Parameswaran, P.; Stoltzfus, J.; Westerhoff, P.; Rittmann, B. E. Total Value of Phosphorus Recovery. *Environ. Sci. Technol.* **2016**, *50* (13), 6606−6620.

(15) Kekedy-Nagy, L.; Abolhassani, M.; Bakovic, S. I. P.; Anari, Z.; Moore, J. P.; Pollet, B. G.; Greenlee, L. F. Electroless Production of Fertilizer (Struvite) and Hydrogen from Synthetic Agricultural Wastewaters. *J. Am. Chem. Soc.* **2020**, *142* (44), 18844−18858.

(16) Prywer, J.; Torzewska, A. Bacterially Induced Struvite Growth from Synthetic Urine: Experimental and Theoretical Characterization of Crystal Morphology. *Cryst. Growth Des.* **2009**, *9* (8), 3538−3543.

(17) Griffith, D. P.; Musher, D. M.; Itin, C. Urease-Primary Cause of Infection-Induced Urinary Stones. *Investigative Urology* **1976**, *13* (5), 346−350.

(18) Bichler, K. H.; Eipper, E.; Naber, K.; Braun, V.; Zimmermann, R.; Lahme, S. Urinary infection stones. *Int. J. Antimicrob. Agents* **2002**, *19* (6), 488−498.

(19) Dogan, S.; Fong, H.; Yucesoy, D. T.; Cousin, T.; Gresswell, C.; Dag, S.; Huang, G.; Sarikaya, M. Biomimetic Tooth Repair: Amelogenin-Derived Peptide Enables in Vitro Remineralization of Human Enamel. *Acs Biomaterials Science & Engineering* **2018**, *4* (5), 1788−1796.

(20) Hostert, J. D.; Kamlet, O.; Su, Z. H.; Kane, N. S.; Renner, J. N. Exploring the effect of a peptide additive on struvite formation and morphology: a high-throughput method. *RSC Adv.* **2020**, *10* (64), 39328−39337.

(21) Li, H.; Yao, Q. Z.; Wang, Y. Y.; Li, Y. L.; Zhou, G. T. Biomimetic synthesis of struvite with biogenic morphology and implication for pathological biomineralization. *Sci. Rep.* **2015**, *5*, 1−8.

(22) Li, H.; Yao, Q. Z.; Yu, S. H.; Huang, Y. R.; Chen, X. D.; Fu, S. Q.; Zhou, G. T. Bacterially mediated morphogenesis of struvite and its implication for phosphorus recovery. *Am. Mineral.* **2017**, *102* (1−2), 381−390.

(23) Rice, J. J.; Daugherty, P. S. Directed evolution of a biterminal bacterial display scaffold enhances the display of diverse peptides. *Protein Engineering Design & Selection* **2008**, *21* (7), 435−442.

(24) Dong, H.; Sarkes, D. A.; Rice, J. J.; Hurley, M. M.; Fu, A. J. Stratis-Cullum, D. N. Living Bacteria−Nanoparticle Hybrids Mediated through Surface-Displayed Peptides. *Langmuir* **2018**, *34* (20), 5837−5848.

(25) Kenrick, S. A.; Daugherty, P. S. Bacterial display enables efficient and quantitative peptide affinity maturation. *Protein Engineering Design & Selection* **2010**, *23* (1), 9−17.

(26) Jahnke, J. P.; Sarkes, D. A.; Liba, J. L.; Sumner, J. J.; Stratis-Cullum, D. N. Improved Microbial Fuel Cell Performance by Engineering E. coli for Enhanced Affinity to Gold. *Energies* **2021**, *14* (17), 5389.

(27) Kirinovic, E.; Leichtfuss, A. R.; Navizaga, C.; Zhang, H. Y.; Christus, J. D. S.; Baltrusaitis, J. Spectroscopic and Microscopic Identification of the Reaction Products and Intermediates during the Struvite (MgNH4PO4 center dot 6H(2) O) Formation from Magnesium Oxide (MgO) and Magnesium Carbonate (MgCO3) Microparticles. *ACS Sustainable Chemistry & Engineering* **2017**, *5* (2), 1567−1577.

(28) Polat, S.; Sayan, P. Preparation, characterization and kinetic evaluation of struvite in various carboxylic acids. *J. Cryst. Growth* **2020**, *531*, 125339.

https://doi.org/10.1021/acsmaterialsau.3c00037
ACS Mater. Au 2023, 3, 548−556

(29) Ye, Z. L.; Chen, S. H.; Lu, M.; Shi, J. W.; Lin, L. F.; Wang, S. M. Recovering phosphorus as struvite from the digested swine wastewater with bittern as a magnesium source. *Water Sci. Technol.* **2011**, *64* (2), 334−340.
(30) Sinha, A.; Singh, A.; Kumar, S.; Khare, S. K.; Ramanan, A. Microbial mineralization of struvite: A promising process to overcome phosphate sequestering crisis. *Water Res.* **2014**, *54*, 33−43.
(31) Rabinovich, A.; Rouff, A. A.; Lew, B.; Ramlogan, M. V. Aerated Fluidized Bed Treatment for Phosphate Recovery from Dairy and Swine Wastewater. *Acs Sustainable Chemistry & Engineering* **2018**, *6* (1), 652−659.
(32) Lafuente, B.; Downs, R. T.; Yang, H.; Stone, N. The power of databases: The RRUFF project. *Highlights in Mineralogical Crystallography* **2015**, 1−29.
(33) Goldstein, J. I.; Newbury, D. E.; Michael, J. R.; Ritchie, N. W. M.; Scott, J. H. J.; Joy, D. C. *Scanning Electron Microscopy and X-Ray Microanalysis*; Springer Science+Business Media LLC: New York, 2017.
(34) Shaddel, S.; Ucar, S.; Andreassen, J. P.; Osterhus, S. W. Engineering of struvite crystals by regulating supersaturation - Correlation with phosphorus recovery, crystal morphology and process efficiency. *Journal of Environmental Chemical Engineering* **2019**, *7* (1), 102918.
(35) Babic-Ivancic, V.; Kontrec, J.; Kralj, D.; Brecevic, L. Precipitation diagrams of struvite and dissolution kinetics of different struvite morphologies. *Croatica Chem. Acta* **2002**, *75* (1), 89−106.
(36) Prywer, J.; Torzewska, A.; Plocinski, T. Unique surface and internal structure of struvite crystals formed by Proteus mirabilis. *Urological Research* **2012**, *40* (6), 699−707.
(37) Prywer, J.; Torzewska, A. Biomineralization of struvite crystals by Proteus mirabilis from artificial urine and their mesoscopic structure. *Crystal Research and Technology* **2010**, *45* (12), 1283−1289.
(38) Luo, Y.; Li, H.; Huang, Y. R.; Zhao, T. L.; Yao, Q. Z.; Fu, S. Q.; Zhou, G. T. Bacterial mineralization of struvite using MgO as magnesium source and its potential for nutrient recovery. *Chem. Eng. J.* **2018**, *351*, 195−202.
(39) Rabinovich, A.; Rouff, A. A. Changes to Struvite Growth and Morphology as Impacted by Low Molecular Weight Organics. *ACS ES&T Water* **2023**, DOI: 10.1021/acsestwater.3c00062, . In press.
(40) Kekedy-Nagy, L.; Teymouri, A.; Herring, A. M.; Greenlee, L. F. Electrochemical removal and recovery of phosphorus as struvite in an acidic environment using pure magnesium vs. the AZ31 magnesium alloy as the anode. *Chem. Eng. J.* **2020**, *380*, 122480.

https://doi.org/10.1021/acsmaterialsau.3c00037
ACS Mater. Au 2023, 3, 548−556